The Cryosphere
Discussions

Open Access

Diagnostic and model dependent uncertainty of simulated Tibetan permafrost area

W. Wang[1], A. Rinke[1,2], J. C. Moore[1], X. Cui[1], D. Ji[1], Q. Li[3], N. Zhang[3], C. Wang[4], S. Zhang[5], D. M. Lawrence[6], A. D. McGuire[7], W. Zhang[8], C. Delire[9], C. Koven[10], K. Saito[11], A. MacDougall[12], E. Burke[13], and B. Decharme[9]

[1]State Key Laboratory of Earth Surface Processes and Resource Ecology, College of Global Change and Earth System Science, Beijing Normal University, Beijing 100875, China
[2]Alfred Wegener Institute Helmholtz Centre for Polar and Marine Research, Potsdam, Germany
[3]Institute of Atmospheric Physics, Chinese Academy of Sciences, Beijing, China
[4]School of Atmospheric Sciences, Lanzhou University, Lanzhou, China
[5]College of Urban and Environmental Sciences, Northwest University, Xi' an, China
[6]NCAR, Boulder, USA
[7]US Geological Survey, Alaska Cooperative Fish and Wildlife Research Unit, University of Alaska, Fairbanks, USA
[8]Department of Physical Geography and Ecosystem Science, Lund University, Lund, Sweden
[9]GAME, Unité mixte de recherche CNRS/Meteo-France, Toulouse CEDEX, France

Title Page

Abstract	Introduction
Conclusions	References
Tables	Figures

|◀ | ▶|
◀ | ▶
Back | Close

Full Screen / Esc

Printer-friendly Version

Interactive Discussion

[10]Lawrence Berkeley National Laboratory, Berkeley, CA, USA
[11]Research Institute for Global Change, Japan Agency for Marine-Earth Science and Technology, Yokohama, Kanagawa, Japan
[12]School of Earth and Ocean Sciences, University of Victoria, Victoria, BC, Canada
[13]Met Office Hadley Centre, Exeter, UK

Correspondence to: X. Cui (xuefeng.cui@bnu.edu.cn)

Title Page

Abstract | Introduction

Conclusions | References

Tables | Figures

|◄ | ►|

◄ | ►

Back | Close

Full Screen / Esc

Printer-friendly Version

Interactive Discussion

Abstract

We perform a land surface model intercomparison to investigate how the simulation of permafrost area on the Tibetan Plateau (TP) varies between 6 modern stand-alone land surface models (CLM4.5, CoLM, ISBA, JULES, LPJ-GUESS, UVic). We also examine the variability in simulated permafrost area and distribution introduced by 5 different methods of diagnosing permafrost (from modeled monthly ground temperature, mean annual ground and air temperatures, air and surface frost indexes). There is good agreement ($99–135 \times 10^4$ km^2) between the two diagnostic methods based on air temperature which are also consistent with the best current observation-based estimate of actual permafrost area (101×10^4 km^2). However the uncertainty ($1–128 \times 10^4$ km^2) using the three methods that require simulation of ground temperature is much greater. Moreover simulated permafrost distribution on TP is generally only fair to poor for these three methods (diagnosis of permafrost from monthly, and mean annual ground temperature, and surface frost index), while permafrost distribution using air temperature based methods is generally good. Model evaluation at field sites highlights specific problems in process simulations likely related to soil texture specification and snow cover. Models are particularly poor at simulating permafrost distribution using definition that soil temperature remains at or below 0°C for 24 consecutive months, which requires reliable simulation of both mean annual ground temperatures and seasonal cycle, and hence is relatively demanding. Although models can produce better permafrost maps using mean annual ground temperature and surface frost index, analysis of simulated soil temperature profiles reveals substantial biases. The current generation of land surface models need to reduce biases in simulated soil temperature profiles before reliable contemporary permafrost maps and predictions of changes in permafrost distribution can be made for the Tibetan Plateau.

1 Introduction

The Tibetan Plateau (TP) has the highest and largest low-latitude frozen ground in the world, with more than 50 % of its area occupied by permafrost (Zhou et al., 2000). The unique geography makes the permafrost on TP very different from the Arctic. The TP permafrost is warmer, with only discontinuous and sporadic permafrost (Zhou et al., 2000), has less underground ice (Ran et al., 2012), and has no large forests (Wu, 1980). The active layer thickness ranges from 1 to 3 m, with some intensely degraded area reaching 4.5 m (Wu and Liu, 2004; Wu and Zhang, 2010; Zhang and Wu, 2012). Freeze/thaw cycles, and the extent of permafrost plays an important role in the thermal state of TP. The temperature contrast between TP and Indian Ocean is an important controlling factor for both the Asian monsoon, and the wider general atmospheric circulation (Xin et al., 2012). As TP gets intensely warmer (IPCC, 2013; Wu et al., 2013), the impact of degraded permafrost on desertification (Li et al., 2014; Yang et al., 2010; Li et al., 2005), water cycling (Cheng and Jin, 2013; Yao et al., 2013), carbon budget (Dörfer et al., 2013; Wang et al., 2008; Schuur et al., 2008;), and infrastructure (Wu and Niu, 2013; Yu et al., 2013) has also become active research topics.

Hence, the simulation of TP permafrost is motivated both by its global importance and by its unique properties. A number of land surface models (LSMs) (e.g., CLM4.0, CoLM, SHAW, Couple Model, FSM and VIC) have been applied at individual station locations to reproduce soil thermo-hydro dynamics (Li et al., 2009; Wang and Shi, 2007; Xiong et al., 2014; Zhang et al., 2012). Simulations of ground temperature and moisture variations are relatively realistic when using observed atmospheric forcing (Guo and Yang, 2010; Luo et al., 2008). The results were improved by setting appropriate permafrost parameters for soil organic matter contents and soil texture properties (Luo et al., 2008; Wang et al., 2007; Xiong et al., 2014). CLM4.0 has also been used to provide future projections of permafrost extent for the whole TP (Guo and Wang, 2013; Guo et al., 2012), and simulates 81 % loss of permafrost area by the end of 21st cen-

tury under the A1B greenhouse gas emissions scenario. This raises the question of how reliable the estimate is in comparison with results from other models.

Simulations of Northern Hemisphere (NH) permafrost area showed large differences amongst Coupled Model Inter-comparison Project (CMIP5) models (Koven et al., 2013; Slater and Lawrence, 2013). Moreover, different diagnostic methods, using either a direct method, which relies on model simulated ground temperatures, or indirect methods inferred from air temperatures and snow characteristics also lead to quite different permafrost areas. Slater and Lawrence (2013) applied two direct methods to nineteen CMIP5 models and found differences of up to 12.6×10^6 km^2 in diagnosed NH permafrost area. Saito (2013) showed that differences in pre-industrial NH continuous permafrost area between direct and indirect methods were around 3×10^6 km^2. This raises the question why different methods arrive at different estimates and which method is better suited.

A reliable simulation of permafrost extent is important, since permafrost is a comprehensive reflection of soil thermo-hydro dynamics that is hard to measure directly except at sparse observational sites. Further, reliable present-day simulations can contribute to an increased confidence in simulations of future permafrost degradation by these models. We note that this approach provides information on the ability of models to simulate permafrost in a region that is both warmer and physically different from where they were "tuned", hence providing some test of reliability for simulations of present and future global permafrost over TP.

To date, an examination of the uncertainties in model-derived TP permafrost area has not been attempted. One way of estimating this uncertainty is to explore a single model and to perform a set of sensitivity experiments in which the model parameters are modified (e.g., Dankers et al., 2011; Essery et al., 2013; Gubler et al., 2013). An alternative approach is to explore an ensemble of multiple models where the uncertainty is discussed in terms of the spread among the models (e.g., Koven et al., 2013; Slater and Lawrence, 2013). Here we follow the second approach and examine the uncertainty of TP permafrost simulations by an ensemble of 6 state-of-the-art stand-

alone land-surface schemes. The models are from the Permafrost Carbon Research Network (Permafrost-RCN; http://www.permafrostcarbon.org/) and include a broad variety of snow and ground parameters and descriptions, along with a clear experimental design under prescribed observation-based atmospheric forcing. The first focus of our paper is therefore the quantification of the uncertainty in the simulated TP permafrost area due to the model's structural and parametric differences. Further, using time series of soil temperature from the few available TP stations, we discuss the biases in relation to the land surface model description (e.g. soil texture, vegetation and snow cover). We also discuss in the paper the uncertainty due to the different methods to diagnose the TP permafrost area, with 5 different (direct and indirect) methods.

In Sect. 2 we introduce the different methods used to derive permafrost extent for the TP from LSMs. Section 3 describes the applied model data, the observation-based estimate of TP permafrost map, the method to assess the agreement of simulated vs. observation-based estimate of permafrost maps, and ground temperature data to evaluate soil thermal profiles simulated by the models. Results and discussion are presented in Sects. 4 and 5, and conclusions are summarized in Sect. 6.

2 Permafrost diagnosis

We make use of all five major permafrost diagnostic methods promoted in the literature. Since the model intercomparison relies on LSMs that are all driven at monthly resolution, the methods we use are tailored, as usual, to reflect the forcing data resolution. The model-derived TP permafrost maps are shown in Fig. 1. The modeling spatial domain is not consistent among the models. CLM4.5, CoLM, JULES and UVic cover the whole TP while others (ISBA, LPJ-GUESS) do not (Table 1). We mainly focus on the common modeling region (Fig. 1) to discuss differences between models and methods, but also give the results for whole TP for the four models that produce them.

In detail, the five methods are:

1. Temperature in Soil Layers (TSL) The TSL method allows a direct diagnosis of permafrost from modeled soil temperature (Slater and Lawrence, 2013). The standard definition of permafrost is that ground remains at or below 0 °C for at least two consecutive years. Many recent modeling studies (e.g., Guo et al., 2012; Guo and Wang, 2013; Slater and Lawrence, 2013 and references therein), have consistently adapted this for land surface and earth system models by defining a model grid cell as permafrost if the simulated ground temperature (of at least one level in the upper soil) remain at or below 0 °C for at least 24 consecutive months. Furthermore, these model studies are limited by the maximum soil depth of the models (Table 1). Hence, we analyze the ground temperatures down to a depth of 3 m, which should be satisfactory as this range spans the observed active layer thickness on TP. Since the models do not provide ground temperatures at a higher temporal resolution than the monthly time scale, the TSL diagnosis is calculated from monthly mean soil temperatures, which has been previously demonstrated to be a viable substitute for model-based estimates of permafrost both on TP (Guo et al., 2012; Guo and Wang, 2013), and for the Arctic (Slater and Lawrence, 2013).

2. Mean Annual Ground Temperature (MAGT)

    Permafrost is detected if the mean annual ground temperature at the depth of zero annual amplitude is at or below 0 °C (Slater and Lawrence, 2013). Some papers use a slightly higher critical temperature, e.g. 0.5 °C (Wang et al., 2006; Wang, 2010; Nan et al., 2002), which has been found to fit TP observations well. Slater and Lawrence (2013) suggested MAGT as an indicator of deeper permafrost. The problem with this definition is that many models have quite shallow soil depth (Table 1), and of course, zero amplitude would require great (actually infinite in steady state) soil depth. For practical purposes, we use MAGT at 3 m depth (the approximate base of the active layer) and the common critical temperature of

0 °C. Although annual ground temperature amplitudes at 3 m depth are still several degrees, they are much smaller than the amplitudes in upper layers (Sect. 4.3). We investigated one model with a larger depth range (CLM4.5; Table 1) in more detail, but found that the results using MAGT at 38 m depth do not significantly change the derived permafrost area.

3. Surface frost index (SFI)

Originally, Nelson and Outcalt (1987) introduced the surface frost index SFI[*], also used in Slater and Lawrence (2013):

$$SFI^* = \frac{\sqrt{DDF_a^*}}{\sqrt{DDF_a^*} + \sqrt{DDT_a}}, \tag{1}$$

where DDF_a^* and DDT_a are the annual freezing and thawing degree-day sums, both calculated using air temperature (indicated by subscript a), and with DDF_a^* further modified to correct for the insulating effect of snow cover (indicated by the *superscript). In this way, SFI[*] is designed to reflect the ground surface thermal conditions by combining snow insulation effect with air temperature. However, the snow insulation effect alone can not account for the soil structure complexity. So here we calculate surface frost index directly from the ground surface temperature (indicated by s subscripts) (Nan et al., 2012), using an asymmetric sinusoidal annual temperature cycle fitted to the warmest and coldest monthly temperatures $(\overline{T_h}, \overline{T_c})$ and a frost angle (β) (Nan et al., 2012):

$$SFI = \frac{\sqrt{DDF_s}}{\sqrt{DDF_s} + \sqrt{DDT_s}} = \frac{1}{1 + \sqrt{\frac{\beta(\overline{T_h}+\overline{T_c})+(\overline{T_h}-\overline{T_c})\sin\beta}{(\beta-\pi)(\overline{T_h}+\overline{T_c})+(\overline{T_h}-\overline{T_c})\sin\beta}}}, \tag{2}$$

Nan et al. (2012) report good results using this surface frost index on TP with values of SFI $\geq$ 0.5 to indicate permafrost.

Title Page

Abstract | Introduction

Conclusions | References

Tables | Figures

◄ | ►

◄ | ►

Back | Close

Full Screen / Esc

Printer-friendly Version

Interactive Discussion

4. Air frost index (F)

Nelson (1987) calculated F from an equation analogous to Eq. (2), but using monthly air temperature rather than ground surface temperatures. Where $F \geq 0.5$ defines permafrost. We follow suit and use F to assess the effects of air temperature forcing. Although many authors have criticized F as a permafrost indicator, F has been used in recent work, though in modified forms. For example, Saito (2013) calculated mean annual air temperature (MAAT) as MAAT = $(DDT_a - DDF_a)/365$, where DDT_a and DDF_a, are thawing index and freezing index as defined earlier which means that MAAT in Saito (2013) is a proxy for F.

5. Mean Annual Air Temperature (MAAT)

A critical value of MAAT is often used to derive the southern boundary of permafrost (Ran et al., 2012; Wang et al., 2006; Jin et al., 2007). The $-2\,°C$ isotherm of MAAT has been found to fit well with TP observation-based permafrost maps (Xu et al., 2001). MAAT has been used to compare the air temperature based permafrost area with permafrost areas derived by other methods (Koven et al., 2013; Saito et al., 2013). Note that the calculation method of MAAT in Saito et al. (2013) is slightly different from that used in other works. Here we calculated MAAT traditionally, as the average of 12 monthly 2 m air temperatures.

All the 5 diagnostic methods are summarized in Table 2. The three direct methods (TSL, MAGT, SFI) are based on simulated ground temperatures, while the two indirect methods (F and MAAT) use the prescribed air temperature. SFI is mainly controlled by air temperature and snow cover, but it also depends on how the soil is parameterized, so SFI is somewhat closer to the indirect methods than are TSL and MAGT.

The 3 methods introduced in the 1980s (SFI, F, MAAT), were designed to map permafrost based on the assumption that the permafrost distribution is related to climatic parameters. Although permafrost processes are directly represented in climate models nowadays, the simulated soil temperatures have considerable errors, and the directly diagnosed permafrost area has model-dependent biases (Koven et al., 2013; Slater

and Lawrence, 2013). Therefore the older indirect diagnostic methods are also still very commonly used (e.g., Wang et al., 2006; Jin et al., 2007; Ran et al., 2012; Nan et al., 2012; Slater and Lawrence, 2013; Saito, 2013; Koven et al., 2013). TP permafrost area directly diagnosed from the simulated monthly soil temperatures (TSL) is not supe-
5 rior to the other methods in comparison with the observation-derived permafrost map (Figs. 1 and 2). Hence, we consider all the 5 diagnostic methods to quantify the full range of uncertainty in the model-derived permafrost maps.

Since the forcing air temperatures of LSMs were not the same due to discrepancies in the historical temperature (and precipitation and other forcing fields) datasets used
10 by the individual models (Table 1), we use the indirect methods to quantify forcing differences. If these differences are not too large, we can attribute the differences in the direct method-derived permafrost areas primarily to differences of modeled land surface processes. Across-model and across-method variability is listed in Table 3. As we use fairly small numbers of methods and models, rather than defining uncertainty in
15 terms of SD, we choose to use the full range of values from the simulations and define uncertainty as maximum-minimum values among the models.

3 Data and analysis approach

3.1 Data from stand-alone LSMs

Output from six stand-alone LSMs participating in the inter-model comparison
20 project "Vulnerability of Permafrost Carbon Research Coordination Network (RCN-Permafrost)" (http://www.permafrostcarbon.org/) is analyzed in this study (Table 1). The simulations have been generally conducted for recent decades from 1960 to 2009 using monthly resolution climate forcing input data. Each modeling team was free to choose appropriate driving data sets for climate, atmospheric CO_2, N deposition, disturbance,
25 soil texture, etc., as used in their standard modeling system. The LSMs use different horizontal model resolutions and different soil layer divisions (Table 1). We also ana-

lyzed (but do not show here) output from a coupled earth-system model (Miroc-ESM). In contrast with the land surface models we present here, the Miroc-ESM coupled model generates its own air temperatures, which over TP, were 4–8 °C cooler than temperatures in the other driving datasets. This creates issues with other model fields such as snow thickness and albedo which make comparison of permafrost processes more difficult than with the stand-alone LSMs.

Our analysis is based on monthly averages of the driving air temperature and simulated ground temperature. As three models (CoLM, JULES and LPJ-GUESS; Table 1) have shallow soil layers, we restrict our analysis to the common depth range spanning near surface to 3 m. Ground temperatures were interpolated onto the common depths: 0.05, 0.1, 0.2, 0.5, 1, 2, 3 m. Since there is no ground surface temperature output, we extrapolate the below soil temperatures onto the ground surface. Most TP permafrost work has been post-1980 (Guo and Wang, 2013; Nan et al., 2012), so we choose 1980 as the start of the analysis period. The end is limited to the year 2000 by results from the JULES model (Table 1).

3.2   TP permafrost observation-based map

Mapping permafrost on TP is challenging due to absence of field observations, especially in the central and western parts where permafrost is widespread. In practice, permafrost maps on TP have been statistical models based on a compilation of earlier maps, aerial photographs, Landsat images and terrain analysis (Ran et al., 2012; Shi et al., 1988; Li and Cheng, 1996; Nan et al., 2002) as well as on some MAGT and MAAT data from the few long-term monitoring sites (Ran et al., 2012; Wang et al., 2006). The classification and therefore the mapping of TP permafrost is not consistent across the different studies (Ran et al., 2012).

The mostly widely used map by Li and Cheng (1996) has large differences from other maps, and shows excess permafrost in the southeast where permafrost can only exist on extremely cold mountains (Gruber, 2012). The International Permafrost Association (IPA) map (Brown et al., 1997; Heginbottom, 2002) is the most widely used in NH

permafrost analysis. However, the IPA map is not well suited for TP because the data and information in this map is based on the map made by Shi et al. (1988) which has not been updated since.

We use the 1 : 4 000 000 Map of the Glaciers, Frozen Ground and Deserts in China (Wang et al., 2006, hereafter refered to as the "Wang06 map") as the primary reference. The map is based on MAGT (Nan et al., 2002) with 0.5 °C as the boundary between permafrost and seasonally frozen ground. Nan (2002) fitted a multiple linear regression between latitude, altitude and MAGT, from all 76 TP stations having borehole data, and extrapolated this regression to the whole TP with a 1 km resolution DEM to get the MAGT distribution. The Wang06 map was re-gridded to match the different model resolutions and spatial domain (see observation column in Fig. 1), and the different permafrost areas derived from the methods and models are compared with the Wang06 map in Fig. 2.

We emphasize that the Wang06 map is subject to uncertainty as it is based on a relatively sparse set of observations and then statistical extrapolation. Nan et al. (2013) pointed out that permafrost was overestimated in the western TP in both the maps by Li and Cheng (1996) and Wang et al. (2006). However, a better permafrost map covering the whole TP is not available.

3.3 Measure of agreement between simulated and Wang06 permafrost maps

To evaluate the agreement of simulated permafrost map with the Wang06 map, we calculate the Kappa coefficient (Cohen, 1960; Monserud and Leemans, 1992; Wang, 2010), K, which measures the degree of agreement between two maps.

$$K = \frac{\left(s/n - (a_1 b_1 + a_0 b_0)/n^2\right)}{\left(1 - (a_1 b_1 + a_0 b_0)/n^2\right)} \tag{3}$$

where the total number of the map points is n, and s is the number of points where simulation and observational estimate agree. The numbers of Wang06 map cells with

permafrost is a_1, and those without are a_0, and the corresponding simulated map cell numbers are b_1 and b_0. The calculated K matrix of simulated and Wang06 permafrost maps is presented in Fig. 3. Empirically, and statistically arbitrary quality values for K have been proposed (e.g. Cohen, 1960), who suggested that $K \geq 0.8$ signifies excellent agreement, $0.6 \leq K < 0.8$ represents substantial agreement, $0.4 \leq K < 0.6$ represents moderate agreement, $0.2 \leq K < 0.4$ represents fair agreement, while lack of agreement corresponds to $K < 0.2$. There is a sample size issue in estimating the confidence of K and this can be a factor when very small numbers of grid points are available (here this applies to UVic).

3.4 Data used to examine model thermal structures

The derived permafrost maps depend on the modeled ground thermal structures. However, field studies on TP are quite limited, and we have only short duration (1996–2000) ground temperature profiles obtained from the GEWEX Asian Monsoon Experiment (GAME)-Tibet (Yang et al., 2003) at three permafrost stations (D66, D105, D110; Fig. 1) in the central TP to compare with model results. We present the top (0.04 m) and deeper (2.63 or 3 m) soil layer temperatures (modeled temperatures were weighted bilinear interpolated onto the station locations) in Fig. 4 and Table 4. We also give a short description of the sites vegetation and soil texture information, both from observation and models.

We also analyze monthly air and ground temperatures in a selected area in the western TP (33–36° N, 82.5–85.5° E, Fig. 1) to examine across-model differences (Fig. 5). As this region is the coldest part of TP (according to the annual mean air temperature) the permafrost is widely distributed, and the active layer thickness is less than 3 m. However, TSL method derived permafrost areas vary significantly among the models in this area (Fig. 1). Despite the lack of any ground temperature observations in this area, the definite presence of permafrost makes it useful to look at the ground thermal structure of each model as well as their differences as a means of interpreting the calculated permafrost areas.

4 Results

4.1 Uncertainties in air-temperature-derived permafrost area

Air temperature–derived permafrost maps are investigated with the two indirect methods, F and MAAT. Figures 1 and 2 compare both Wang06 and model-derived permafrost maps, and show that F produces consistently excessive permafrost area compared with MAAT. That is because the empirical threshold of $-2\,^{\circ}C$ for MAAT fits well with TP observations (Xu et al., 2001), while $F \geq 0.5$ is a theoretical assumption, which has been reported to overestimate permafrost area (Nelson and Outcalt, 1987; Slater and Lawrence, 2013). Accordingly, Fig. 3 shows that F derived permafrost is less consistent with observation (model average $K = 0.3$ for the common region) than MAAT-derived permafrost area ($K = 0.5$).

Across-model variability (Table 3) for the MAAT-based method is $14 \times 10^4\,km^2$ and for the F based method is $17 \times 10^4\,km^2$, equivalent to about 14–17 % of the Wang06 permafrost area inside the common modeling region ($101 \times 10^4\,km^2$). This variability is much smaller than the 56 % calculated by Slater and Lawrence (2013) for the CMIP5 models with the SFI[*] method for NH permafrost area. The relatively smaller difference among the models here is because, although the temperature forcing was not identical among models, the mean annual air temperature and its spatial variability in the permafrost region are quite similar (between -6 and $-8\,^{\circ}C$). Hence most of the differences among the indirect methods that use air temperature to derive permafrost area can be attributed to different model horizontal resolutions. Since the differences in permafrost extent using the air temperature based indirect methods are relatively small, the differences in the direct method derived extents can primarily be attributed to the LSMs structural and parametric differences.

4.2 Uncertainties in model–derived permafrost area

There is a large across-model variability of permafrost area derived from direct methods (TSL, MAGT and SFI) (Figs. 1 and 2; 111–120× 10^4 km^2; Table 3) and it is similar for all the 3 diagnosis methods. This across-model variability is much larger than the variability using the indirect methods discussed in Sect. 4.1, and is equivalent to 110–112 % of Wang06 permafrost area for the common modeling region. CMIP5 across-model variability derived from TSL in NH permafrost area was similarly large (Slater and Lawrence, 2013; Koven, 2013). Clearly this points to large across-model differences in ground thermal structures.

The across-method (TSL, MAGT and SFI) variability in permafrost area (Figs. 1 and 2; Table 3) is very variable between models: UVic and LPJ-GUESS have smallest ranges (up to 9×10^4 km^2), while CoLM has the largest (87×10^4 km^2) (Table 3), near to the total permafrost area of the common region. Thus the across-direct method range is similar to the across-model range. Slater and Lawrence (2013) also emphasized the variable across-method variability for NH permafrost area between models, however Saito (2013) showed insignificant variability across both direct and indirect methods for derived pre-industrial NH continuous permafrost area.

4.3 Model evaluation based on K and ground temperature profile

A good land surface model should adequately simulate the seasonal and annual ground temperature profiles. Hence one quality test for a model is that it should be able to produce "good" permafrost maps, which we define as agreement with the observation-based map, based on all the three direct diagnostic methods. The applied criterion is the kappa coefficient K (Sect. 3.3). If we take the (arbitrary) threshold $K \geq 0.4$ (indicating "moderate agreement"), then no model passes this test for the common simulation region, while reducing the threshold to $K \geq 0.2$ ("fair agreement") allows most models and methods to pass while UVic stands out as a clear failure (Fig. 3).

If the criterion for acceptable model bias is $\leq \pm 2.0\,^\circ$C, then simulations of mean annual ground temperatures from most models (CLM4.5, CoLM, ISBA and JULES) agree with the observations, but only the simulation of seasonal cycle amplitude of one model (ISBA) agrees with observations. However, if the criterion is bias $\leq \pm 1.0\,^\circ$C, then no model agrees with observations for neither mean annual ground temperature nor the seasonal cycle amplitude (Fig. 4, Table 4).

We now look at the performance of the 2 models with larger biases in mean annual ground temperature: LPJ-GUESS and UVic. LPJ-GUESS simulated too cold (by more than 3 $^\circ$C) mean annual ground temperatures for both the surface and deeper layers (Fig. 4, Table 4). The summer temperatures simulated by the model in the surface layers are especially cold, with maximum temperatures lower than observation by 8 $^\circ$C (Fig. 4a and c) and its ground temperature amplitude is substantially underestimated (Table 4), which must greatly limit the summer thaw depth. This cold soil results in substantial overestimation of permafrost area (119–131 $\times 10^4$ km^2; Table 3, Fig. 2) with small across-method variability.

UVic simulates a soil thermal state that is the warmest among the models, with the simulated mean annual ground temperature at D66 surpassing observation by more than 7 $^\circ$C (Fig. 4, Table 4). If the observational sites are representative then the generally too warm ground temperature in UVic is the reason for the extremely small simulated permafrost area (8 $\times 10^4$ km^2; Table 3, Fig. 2) with all direct methods, and hence to no across-method variability, and poor agreement with the Wang06 permafrost map ($K < 0.1$; Fig. 3).

4.4 Method comparison based on K and ground temperature profile

Permafrost maps derived using MAGT and SFI often show larger area than TSL (Fig. 2), with generally better agreement with the Wang06 map (Fig. 3). The MAGT method simply defines a grid as permafrost as long as its 3 m mean annual ground temperature is colder than 0 $^\circ$C, and a permafrost threshold value of SFI $\geq$ 0.5 also only requires the mean annual ground surface temperature is lower than 0 $^\circ$C (Nan,

2012). Figures 4 and 5 show most models meet these criteria. However, assuming that the site observations are representative, the simulated mean annual ground temperatures of both surface and deeper soil layers often have obvious biases ($\geq \pm 1\,°C$) in all the models (Fig. 4 and Table 4).

In general, model-derived permafrost distribution using the TSL method shows little agreement with the Wang06 map (Figs. 1–3). In contrast with MAGT and SFI methods, the TSL method requires adequate simulation of both mean annual ground temperature and the seasonal cycle at monthly resolution (Fig. 4, Table 4). This means that the TSL method is more susceptible to model errors, but it offers a more comprehensive insight into land model processes. CoLM is an extreme example of how a simulated permafrost map can be totally incorrect due to small errors in seasonal ground temperature. CoLM simulates nearly no TSL -derived permafrost (Figs. 1 and 2), accounting for much of the large across-model and across-method variability (Table 3). This is despite CoLM having lower mean annual ground temperatures for the 3 m layer than many other models (ISBA, CLM4.5 and JULES). However, it simulates a larger seasonal amplitude than CLM4.5 and ISBA (Fig. 5), so that, in the western TP, the monthly maximum 3 m ground temperatures in CoLM always surpasses $0\,°C$ by around $0.2\,°C$ (Fig. 5c) precluding it being classed as permafrost with the TSL method.

5 Discussion of the related main processes causing ground temperature discrepancies

In comparison with site observations, the most noticeable ground temperature discrepancies of the 6 models discussed in Sect. 4 and relevant for the most biased simulated permafrost area are the underestimation of soil temperature by LPJ-GUESS and the overestimation of soil temperature by UVic. There are many other, rather subtle, potential model discrepancies that we do not investigate in detail here. One example is the overestimation of the amplitude of the seasonal temperature cycle at deep depths in several models (Fig. 4b and d; Table 4). Table 4 also shows that the observed vegeta-

tion and soil texture are mis-matched by all the models at each of the stations. Although it is a common problem to compare grid cell results against site data, model description of vegetation and soil texture is too simplified.

To help elucidate the causes of ground temperature discrepancies associated with soil processes we also inspect snow depth and vertical ground temperature gradients. We use the Long Time Series Snow Dataset of China (Che et al., 2008) (http://westdc.westgis.ac.cn) to examine the modeled snow depth. The complete dataset is composed of SMMR (1978–1987), SSM/I (1987–2008) and AMSR-E (2002–2010). Here we use the data of SMMR and SSM/I to produce the winter (DJF) climatological distribution of 1980–2000 (Fig. 6). Furthermore, we follow Koven et al. (2013) and calculated two vertical gradients to isolate processes: from the atmosphere to ground surface (Fig. 7) and from ground surface to deeper soil (at 1 m depth) (Fig. 8). While the first one is mainly controlled by the snow insulation, the latter is mainly determined by soil hydrology, latent heat and thermal properties. Important factors that influence the ground thermal structure are compared in Table 5. Since several models produce incomplete or not directly comparable output, we restrict ourselves to a qualitative assessment here.

The LPJ-GUESS simulated underestimation of soil temperature is not caused by a bias in the surface air temperature forcing (Fig. 5, Table 4). Instead, this bias may be due to many factors such as inappropriate prescriptions of soil thermal properties, poor representation of soil hydrology, and mis-match of vegetation types. Figure 8 shows that the soil temperatures increase with depth, but LPJ-GUESS has a much smaller temperature gradient between the surface and the 1 m deep soil (0–2 K) than the other models. This suggests a different (larger) winter soil thermal conductivity probably associated with a high soil porosity and water content. LPJ-GUESS specifies the same soil texture for the TP as for the Arctic, which is mostly clay-like (Table 4). Clay has high water retention capacity. Many studies have reported that the soil on TP is immature, with coarser particles than typical for Arctic permafrost and with much less organic matter. Inappropriate soil texture classification will affect the simulated ground thermal

structure. LPJ-GUESS underestimates the surface and top soil temperatures particularly in summer (Figs. 4a and c, 5). Precipitation and hydrological processes determine the vertical profile of soil water content which can change the fraction of water and ice retained in different soil layers and influence soil thermal conduction. The energy required to melt the high water (ice) content in the surface soil layers in summer appears to lead underestimated low summer temperatures compared with other models, and a phase lag in summer warming (Fig. 4a and c).

UVic uses the same climate forcing as CLM4.5 (Table 1), but simulates much warmer ground temperatures than other models. In contrast with the other models, UVic has no snow cover in winter (Fig. 6), which is consistent with grid cell surface albedo being year-round at values between 0.15–0.35. The simulated snow depth is derived from the prescribed winter precipitation, and the model's snow, energy and water balances. The lack of snow over TP in UVic likely indicates removal by sublimation. A too low snow albedo makes the snow gain energy that is lost through sublimation. Since it takes more energy to sublimate snow than it does to melt it, the latent heat flux should be, and is (not shown) higher in UVic than other models. However, despite the apparent snow sublimation – which should cool the soil, the ground surface temperatures in UVic are warmer than in all the models. The large absorption of short wave radiation allowed by the year-round low albedo provides this heat and is sufficient for there to be very little permafrost simulated by UVic for the TP.

ISBA, and especially JULES stand out from other models in their calculated winter temperature offsets: ground surface temperatures are colder than the driving air temperatures over much of the simulated region (Fig. 7), and in those places the deep soil temperatures are relatively warmer (Fig. 8). Snow (Fig. 6) and vegetation cover should provide insulation making soil warmer than air temperatures in winter, thus the negative temperature offsets are not physically consistent. Snow depth for the two models is thick enough to produce a warming effect (Fig. 6). This suggests problems with surface insulation which, to a degree, is compensated for by an anomalous soil thermal conductivity that maintains deep soil warmth in those regions with a negative insulation

Diagnostic and model dependent uncertainty of simulated Tibetan permafrost area

W. Wang et al.

Title Page

Abstract	Introduction
Conclusions	References
Tables	Figures

|◄ | ►|

◄ | ►

Back | Close

Full Screen / Esc

Printer-friendly Version

Interactive Discussion

effect. Hence, although the permafrost maps produced by the models have a $K > 0.2$ compared with the observation-based Wang06 map, there are problems with the surface and soil temperature profiles.

6   Summary and conclusions

Results of this model intercomparison quantify, for the first time, the uncertainties of model derived permafrost area on the Tibetan Plateau (TP). The uncertainties stem from across-model and across-diagnostic method variability as well as historic climate data uncertainties. According to the agreement of the air temperature based diagnostic methods (MAAT and F), we found lower uncertainty in permafrost area associated with air temperature forcing ($99\text{–}135 \times 10^4$ km^2) in comparison with the uncertainty ($1\text{–}128 \times 10^4$ km^2) associated with the simulation of soil temperature used in the other three diagnostic methods (TSL, MAGT, and SFI); observation-based Wang06 permafrost area is 101×10^4 km^2.

The models in this study generally produced permafrost maps in better agreement with the Wang06 map using the MAGT and SFI methods rather than with the TSL method. But this does not mean that the models simulate permafrost dynamics correctly. Although most models can capture the threshold value of MAGT and SFI, their ground temperatures still show various biases, both in the mean annual value and the seasonal variation. Therefore, most models produce worse permafrost maps with the TSL method. The TSL method is a more demanding, and to date, elusive target.

Modeled snow depth and surface and soil temperature offsets vary widely amongst the models. If the observation sites for soil temperature are representative, then LPJ-GUESS and UVic have substantial biases in their soil temperature simulations, mainly attributable to inappropriate description of the surface (vegetation, snow cover) and soil properties (soil texture, hydrology). Other models (ISBA, JULES) show biases in the simulation of winter soil temperature.

From investigations in the arctic and boreal regions, we know that the specification of surface and soil properties needs substantial improvement. In addition, models need to consider deeper soil columns in their simulations. Nicolsky et al. (2007) recommend a soil column of at least 80 m for models applied to arctic and boreal regions. The permafrost in the TP is usually much warmer and with a deeper active layer than found in continuous permafrost of the arctic and boreal region, hence deep soil layers would also be applicable for TP permafrost simulation. A shallow column in a permafrost model can cause problems in the simulation of the degradation of warm permafrost (near 0 °C), which is expected for projections of future climate warming (Alexeev et al., 2007; Lawrence et al., 2008).

Further evaluation of model results from the permafrost-RCN is underway for TP that examines permafrost temperature, active layer thickness and carbon balance under present and future climate forcing. We also plan to complement this model intercomparison study by an uncertainty quantification analysis of key model parameters (e.g. improved vegetation and snow albedo, soil colors, etc) with the CoLM model. However, a crucial requirement for this is much better data availability allowing for better spatial coverage across the TP in the evaluation of simulated ground temperature profiles. Under the Chinese Scientific Foundation Project "Permafrost Background Investigation on the Tibetan Plateau" (No. 2010CB951402), a series of new stations have been established, especially in the depopulated zone. More ground truth data will be published in the near future, which will also be assimilated in a new observation-based permafrost map.

Title Page

Abstract | Introduction

Conclusions | References

Tables | Figures

◄ | ►

Back | Close

Full Screen / Esc

Printer-friendly Version

Interactive Discussion

References

Alexeev, V., Nicolsky, D., Romanovsky, V., and Lawrence, D.: An evaluation of deep soil configurations in the CLM3 for improved representation of permafrost, Geophys. Res. Lett., 34, L09502, doi:10.1029/2007GL029536, 2007.

AWFA: Data Format Handbook for AGRMET, available at: http://www.mmm.ucar.~edu/mm5/documents/data_format_handbook.pdf (last access: 20 January 2010), 2002.

Brown, J., Ferrians, O., Heginbottom, J., and Melnikov, E.: Circum-Arctic Map of Permafrost and Ground-Ice Conditions, US Geological Survey, Reston, USA, 1997.

Che, T., Li, X., Jin, R., Armstrong, R., and Zhang, T. J.: Snow depth derived from passive microwave remote-sensing data in China, Ann. Glaciol., 49, 145–154, 2008.

Cheng, G. and Jin, H.: Permafrost and groundwater on the Qinghai-Tibet Plateau and in northeast China[J], Hydrogeol. J., 21, 5–23, 2013.

Cohen, J.: A coefficient of agreement for nominal scales, Educ. Psychol. Meas., 20, 37–46, 1960.

Dankers, R., Burke, E. J., and Price, J.: Simulation of permafrost and seasonal thaw depth in the JULES land surface scheme, The Cryosphere, 5, 773–790, doi:10.5194/tc-5-773-2011, 2011.

Dörfer, C., Kühn, P., Baumann, F., He, J., and Scholten, T.: Soil organic carbon pools and stocks in permafrost-affected soils on the Tibetan Plateau, PloS One, 8, e57024, doi:10.1371/journal.pone.0057024, 2013.

Essery, R., Morin, S., Lejeune, Y., and Ménard, C. B.: A comparison of 1701 snow models using observations from an alpine site, Adv. Water Resour., 55, 131–148, doi:10.1016/j.advwatres.2012.07.013, 2013.

Gruber, S.: Derivation and analysis of a high-resolution estimate of global permafrost zonation, The Cryosphere, 6, 221–233, doi:10.5194/tc-6-221-2012, 2012.

Gubler, S., Endrizzi, S., Gruber, S., and Purves, R. S.: Sensitivities and uncertainties of modeled ground temperatures in mountain environments, Geosci. Model Dev., 6, 1319–1336, doi:10.5194/gmd-6-1319-2013, 2013.

Title Page

Abstract | Introduction

Conclusions | References

Tables | Figures

|◄ | ►|

◄ | ►

Back | Close

Full Screen / Esc

Printer-friendly Version

Interactive Discussion

Guo, D. and Yang, M.: Simulation of Soil Temperature and Moisture in Seasonally Frozen Ground of Central Tibetan Plateau by SHAW Model, Plateau Meteorology, 29, 1369–1377, 2010.

Guo, D. and Wang, H.: Simulation of permafrost and seasonally frozen ground conditions on the Tibetan Plateau, 1981–2010, J. Geophys. Res.-Atmos., 118, 5216–5230, 2013.

Guo, D., Wang, H., and Li, D.: A projection of permafrost degradation on the Tibetan Plateau during the 21st century, J. Geophys. Res.-Atmos., 117, D05106, doi:10.1029/2011JD016545, 2012.

Heginbottom, J.: Permafrost mapping: a review, Prog. Phys. Geog., 26, 623–642, 2002.

Hillel, D.: Environmental Soil Physics: Fundamentals, Applications, and Environmental Considerations, Academic Press, New York, USA, 1998.

IPCC: Climate Change 2013: the Physical Science Basis Contribution of Working Group I to the Fifth Assessment Report of the Intergovernmental Panel on Climate Change, Cambridge University Press, Cambridge, 2013.

Ji, D., Wang, L., Feng, J., Wu, Q., Cheng, H., Zhang, Q., Yang, J., Dong, W., Dai, Y., Gong, D., Zhang, R.-H., Wang, X., Liu, J., Moore, J. C., Chen, D., and Zhou, M.: Description and basic evaluation of Beijing Normal University Earth System Model (BNU-ESM) version 1, Geosci. Model Dev., 7, 2039–2064, doi:10.5194/gmd-7-2039-2014, 2014.

Jin, H., Yu, Q., Lü, L., Guo, D., He, R., Yu, S., Sun, G., and Li, Y.: Degradation of permafrost in the Xing'anling Mountains, Northeastern China, Permafrost Periglac., 18, 245–258, 2007.

Koven, C., Riley, W., and Stern, A.: Analysis of permafrost thermal dynamics and response to climate change in the CMIP5 Earth System Models, J. Climate, 26, 1877–1900, 2013.

Lawrence, D. and Slater, A.: A projection of severe near-surface permafrost degradation during the 21st century, Geophys. Res. Lett., 32, L24401, doi:10.1029/2005GL025080, 2005.

Lawrence, D., Slater, A., Romanovsky, V., and Nicolsky, D.: The sensitivity of a model projection of near-surface permafrost degradation to soil column depth and inclusion of soil organic matter, J. Geophys. Res., 113, F02011, doi:10.1029/2007JF000883, 2008.

Li, Q., Sun, S., and Dai, Q.: The numerical scheme development of a simplified frozen soil model, Adv. Atmos. Sci., 26, 940–950, 2009.

Li, S. and Cheng, G.: Map of Frozen Ground on Qinghai-Xizang Plateau, Gansu Culture Press, Lanzhou, 1996.

Title Page

Abstract | Introduction

Conclusions | References

Tables | Figures

◀ | ▶

◀ | ▶

Back | Close

Full Screen / Esc

Printer-friendly Version

Interactive Discussion

Li, S., Gao, S., Yang, P., and Chen, H.: Some problems of freeze–thaw desertification in the Qinghai-Tibetan Plateau: a case study on the desertification regions in the western and northern Tibet, J. Glaciol. Geocryol., 27, 476–485, 2005.

Li, Z., Tang, P., Zhou, J., Tian, B., Chen, Q., and Fu, S.: Permafrost environment monitoring on the Qinghai-Tibet Plateau using time series ASAR images, International Journal of Digital Earth, doi:10.1080/17538947.2014.923943, online, first, 2014.

Luo, S., Lv, S., Zhang, Y., Hu, Z., Ma, Y., Li, S., and Shang, L.: Simulation analysis on land surface process of BJ site of central Tibetan Plateau using CoLM, Plateau Meteorology, 27, 259–271, 2008.

Monserud, R. and Leemans, R.: Comparing global vegetation maps with the Kappa statistic, Ecol. Model., 62, 275–293, 1992.

Nan, Z., Li, S., and Liu, Y.: Mean annual ground temperature distribution on the Tibetan Plateau: permafrost distribution mapping and further application, J. Glaciol. Geocryol., 24, 142–148, 2002.

Nan, Z., Li, S., Cheng, G., and Huang, P.: Surface frost number model and its application to the Tibetan plateau, J. Glaciol. Geocryol., 34, 89–95, 2012.

Nan, Z., Huang, P., and Zhao, L.: Permafrost distribution modeling and depth estimation in the Western Qinghai-Tibet Plateau, Acta Geographica Sinica, 68, 318–327, 2013.

Nelson, F. and Outcalt, S.: A computational method for prediction and regionalization of permafrost, Arctic Alpine Res., 19, 279–288, 1987.

Nicolsky, D. J., Romanovsky, V. E., Alexeev, V. A., and Lawrence, D. M.: Improved modeling of permafrost dynamics in a GCM land-surface scheme, Geophys. Res. Lett., 34, L08501, doi:10.1029/2007GL029525, 2007.

Qin, J., Yang, K., Liang, S., Zhang, H., Ma, Y., Guo, X., and Chen, Z.: Evaluation of surface albedo from GEWEX-SRB and ISCCP-FD data against validated MODIS product over the Tibetan Plateau, J. Geophys. Res.-Atmos., 116, D24116, doi:10.1029/2011JD015823, 2011.

Ran, Y., Li, X., Cheng, G., Zhang, T., Wu, Q., Jin, H., and Jin, R.: Distribution of permafrost in China: an overview of existing permafrost maps, Permafrost Periglac., 23, 322–333, 2012.

Saito, K., Sueyoshi, T., Marchenko, S., Romanovsky, V., Otto-Bliesner, B., Walsh, J., Bigelow, N., Hendricks, A., and Yoshikawa, K.: LGM permafrost distribution: how well can the latest PMIP multi-model ensembles perform reconstruction?, Clim. Past, 9, 1697–1714, doi:10.5194/cp-9-1697-2013, 2013.

Title Page

Abstract	Introduction
Conclusions	References
Tables	Figures

|◄ | ►|

◄ | ►

Back | Close

Full Screen / Esc

Printer-friendly Version

Interactive Discussion

Schuur, E. A., Bockheim, J., Canadell, J. G., Euskirchen, E., Field, C. B., Goryachkin, S. V., Hagemann, S., Kuhry, P., Lafleur, P. M., and Lee, H.: Vulnerability of permafrost carbon to climate change: implications for the global carbon cycle, BioScience, 58, 701–714, 2008.

Shi, Y., Mi, D., Feng, Q., Li, P., and Wang, Z.: Map of Snow, Ice and Frozen Ground in China, China Cartographic Publishing House, Beijing, China, 1988.

Slater, A. and Lawrence, D.: Diagnosing present and future permafrost from climate models, J. Climate, 26, 5608–5623, doi:10.1175/JCLI-D-12-00341.1, 2013.

Tian, L., Li, W., Zhang, R., Tian, L., Zhu, Q., Peng, C., and Chen, H.: The analysis of snow information from 1979 to 2007 in Qinghai-Tibetan Plateau, Acta Ecologica Sinica, 34, 5974–5983, 2014.

Van, D.: Influence of Soil Management on the Temperature Wave Near the Soil Surface, Tech. Bull. 29, Institute of Land and Water Manage. Res., Wageningen, Netherlands, 21 pp., 1963.

Wang, C. and Shi, R.: Simulation of the land surface processes in the Western Tibetan Plateau in summer, J. Glaciol. Geocryol., 29, 73–81, 2007.

Wang, G., Li, Y., Wang, Y., and Wu, Q.: Effects of permafrost thawing on vegetation and soil carbon pool losses on the Qinghai-Tibet Plateau, China, Geoderma, 143, 143–152, 2008.

Wang, K., Cheng, G., Jiang, C., and Niu, F.: Variation of thermal diffusivity and temperature simulation of soils of vertical heterogeneity in Nagqu Prefecture in the Tibetan Plateau, Journal of Glaciology and Geocryology, 29, 470–474, 2007.

Wang, T., Wang, N. L., and Li, S. X.: Map of the Glaciers, Frozen Ground and Desert in China, 1 : 4 000 000 (in Chinese), Chinese Map Press, Beijing, China, 2006.

Wang, X., Yang, M., and Wan, G.: Processes of soil thawing-freezing and features of ground temperature and moisture at D105 on the Northern Tibetan Plateau, J. Glaciol. Geocryol., 34, 56–63, 2012.

Wang, Z.: Applications of permafrost distribution models on the Qinghai-Tibetan Plateau, Lanzhou University, China, 2010.

Wu, Q. and Liu, Y.: Ground temperature monitoring and its recent change in Qinghai-Tibet Plateau, Cold Reg. Sci. Technol., 38, 85–92, 2004.

Wu, Q. and Niu, F.: Permafrost changes and engineering stability in Qinghai-Xizang Plateau, Chinese Sci. Bull., 58, 1079–1094, 2013.

Wu, Q. and Zhang, T.: Changes in active layer thickness over the Qinghai-Tibetan Plateau from 1995 to 2007, J. Geophys. Res.-Atmos., 115, D09107, doi:10.1029/2009JD012974, 2010.

Wu, T., Zhao, L., Li, R., Wang, Q., Xie, C., and Pang, Q.: Recent ground surface warming and its effects on permafrost on the central Qinghai-Tibet Plateau, Int. J. Climatol., 33, 920–930, 2013.

Xin, Y., Wu, B., Bian, L., Liu, G., Zhang, L., and Li, R.: Simulation study of permafrost hydro–thermo dynamics on Asian climate (in Chinese), in: 29th Annual Meeting of Chinese Metero-logical Society, Shenyang, China, 12 September 2012, P461, 9–12, 2012.

Xiong, J., Zhang, Y., Wang, S., Shang, L., Chen, Y., and Shen, X.: 1. Key Laboratory of Land Surface Process and Climate Change in Cold and Arid Regions, Cold and Arid Regions Environment Research Institute, Chinese Academy of Science, Lanzhou 730000, China; 2. University of Chinese Academy of Sciences, Beijing 100049, China, Plateau Meteorology, 33, 323–336, 2014.

Xu, X. and Lin, Z.: Remote sensing retrieval of surface monthly mean albedo in Qinghai-Xizang Plateau, Plateau Meteorology, 21, 233–237, 2002.

Yao, T., Qin, D., Shen, Y., Zhao, L., Wang, N., and Lu, A.: Cryospheric changes and their impacts on regional water cycle and ecological conditions in the Qinghai Tibetan Plateau, Chinese J. Nature, 35, 179–186, 2013.

Yang, M., Yao, T., and He, Y.: The extreme value analysis of the ground temperature in northern part of Tibetan Plateau records from D110 site, J. Mount. Sci. (China), 17, 207–211, 1999.

Yang, M., Yao, T., and Gou, X.: The freezing thawing processes and hydro-thermal character-istics along the road on the Tibetan Plateau, Advancement of Natural Scinece (China), 10, 443–450, 2000.

Yang, M., Yao, T., Gou, X., Koike, T., and He, Y.: The soil moisture distribution, thawing–freezing processes and their effects on the seasonal transition on the Qinghai-Xizang (Tibetan) plateau, J. Asian Earth Sci., 21, 457–465, doi:10.1016/S1367-9120(02)00069-X, 2003.

Yang, M., Nelson, F., Shiklomanov, N., Guo, D., and Wan, G.: Permafrost degradation and its environmental effects on the Tibetan Plateau: a review of recent research, Earth-Sci. Rev., 103, 31–44, 2010.

Yu, F., Qi, J., Yao, X., and Liu, Y.: In-situ monitoring of settlement at different layers under embankments in permafrost regions on the Qinghai-Tibet Plateau[J], Eng. Geol., 160, 44–53, 2013.

Zhang, W., Wang, G., Zhou, J., Liu, G., and Wang, Y.: Simulating the water-heat processes in permafrost regions in the Tibetan Plateau based on CoupModel, J. Glaciol. Geocryol., 34, 1099–1109, 2012.

Diagnostic and model dependent uncertainty of simulated Tibetan permafrost area

W. Wang et al.

Title Page

Abstract	Introduction
Conclusions	References
Tables	Figures

Back | Close

Full Screen / Esc

Printer-friendly Version

Interactive Discussion

Zhang, Z. and Wu, Q.: Predicting changes of active layer thickness on the Qinghai-Tibet Plateau as climate warming, J. Glaciol. Geocryol., 34, 505–511, 2012.

Zhou, Y., Guo, D., Qiu, G., Cheng, G., and Li, S.: China Permafrost, Science Press, Beijing, China, 232 pp., 2000.

Diagnostic and model dependent uncertainty of simulated Tibetan permafrost area

W. Wang et al.

Table 1. The six land surface models, analyzed over the Tibetan plateau (TP).

Model	Native Resolution	Number of soil layers	Depth of soil column (m)	Spatial domain	Atmospheric Forcing Data
CLM4.5	1° × 1.25°	30	38.1	Whole TP	CRUNCEP4[a]
CoLM	1° × 1°	10	2.86	Whole TP	Princeton[b]
ISBA	0.5° × 0.5°	14	10	Permafrost region follow IPA map	WATCH[c]
JULES	0.5° × 0.5°	30	2.95	Whole TP	WATCH[c]
LPJ-GUESS	0.5° × 0.5°	25	3	Permafrost region follow IPA map	CRU TS 3.1[d]
UVic	1.8° × 3.6°	14	198.1	Whole TP	CRUNCEP4[a]

[a] Viovy and Ciais (http://dods.extra.cea.fr/).
[b] Sheffield et al. (2006) (http://hydrology.princeton.edu/data.pgf.php).
[c] Weedon et al. (2011) (http://www.waterandclimatechange.eu/about/watch-forcing-data-20th-century).
[d] Harris et al. (2013), University of East Anglia Climate Research Unit (2013).

Table 2. The five diagnostic methods to derive permafrost.

Method	Definition	Data used for calculation
TSL	More than 24 consecutive months soil temperature $\leq 0\,°C$	0–3 m monthly soil temperature
MAGT	Mean annual of 3 m soil temperature $\leq 0\,°C$	Mean annual of 3 m soil temperature
SFI	Surface frost number ≥ 0.5	Annually maximum and minimum ground surface temperature
F	Air frost number ≥ 0.5	Annually maximum and minimum air temperature
MAAT	Mean annual air temperature $\leq -2\,°C$	Mean annual of air temperature

Title Page

Abstract | Introduction

Conclusions | References

Tables | Figures

|◄ | ►|

◄ | ►

Back | Close

Full Screen / Esc

Printer-friendly Version

Interactive Discussion

Table 3. Derived permafrost area inside the common modeling region on Tibetan Plateau (10^4 km^2) from 6 LSMs and 5 diagnostic methods.

		CLM4.5	CoLM	JULES	UVic	ISBA	LPJ-GUESS	across-model uncertainty
Indirect method	MAAT	113	105	111	99	109	110	14
	F	135	127	131	118	130	131	17
Direct method	TSL	60	1	62	8	44	119	118
	MAGT	104	88	96	8	61	128	120
	SFI	115	62	100	8	112	119	111
across-direct method uncertainty		55	87	38	0	68	9	

Table 4. Model-observed temperatures differences in mean annual and seasonal cycle amplitude of air and soil temperature, based on data from 1996–2000 (Sect. 3.4; Fig. 4), and the corresponding vegetation and soil properties of both observation and models. Air temperature data is only available for D66 station and limited from 1997/9 to 1998/8. Thus the statistics of ground temperature of D66 is also confined to this period.

	D66 (35.63° N, 93.81° E)								
	Temperature bias "Model-Observation"						Soil conditions		
	Air temperature		Ground temperature						
			0.04 m depth		2.63 m depth		Bare ground	Vegetation	Texture (top soil)
	Mean annual	Seasonal amplitude	Mean annual	Seasonal amplitude	Mean annual	Seasonal amplitude			
Obs[a]	–	–	–	–	–	–	100 %	None	gravel
CLM4.5[b]	4.3	1	2	–0.2	2	3.5	81 %	10 % boreal shrub 8 % C3 arctic grass	63 % sand 19 % clay
CoLM[c]	2.3	0.1	0	0.1	–1	2.4	87 %	4 % boreal shrub 5 % C3 arctic grass 3 % C3 non arctic grass	43 % sand 18 % clay
ISBA[d]	1.4	0.1	–1.3	–1.3	0.8	0.5	53 %	46 % C3 grass	55 % sand 7 % clay
JULES[j]	1.1	0.3	–0.5	2.1	–2	4	–	–	–
LPJ-GUESS[e,i]	1.5	–0.1	–3.4	–6.6	–3.7	1.5	–	tundra	clay-like
UVic[f]	2.6	0.5	7.5	–1.5	7.6	2.1	100 %	None	44 % sand 24 % clay

Table 4. Continued.

	Temperature bias "Model-Observation"		Soil conditions		
	Ground temperature 3 m depth				
	Mean annual	Seasonal amplitude	Bare ground	Vegetation	Texture (top soil)
D105 (33.07° N, 91.94° E)					
Obs[g]	–	–	50–60 %	grass (Leontopodium nanum)	coarse and fine sand
CLM4.5[b]	−1.2	0.8	48 %	17 % boreal_shrub 30 % C3 arctic grass	60 % sand 20 % clay
CoLM[c]	0.1	0.2	7 %	69 % C3 arctic grass 24 % C3 non arctic grass	38 % sand 16 % clay
ISBA[d]	0.9	−0.9	27 %	72 % C3 grass	52 % sand 10 % clay
JULES[j]	−1.8	1.8	–	–	–
LPJ -GUESS[e,i]	−3.7	0.7	–	tundra	clay-like
UVic[f]	1	−0.2	7 %	33 % C3 grass 60 % shrub	43 % sand 32 % clay

Title Page

Abstract   Introduction

Conclusions   References

Tables   Figures

◄   ►

Back   Close

Full Screen / Esc

Printer-friendly Version

Interactive Discussion

Table 4. Continued.

	Temperature bias "Model-Observation"		Soil conditions		
	Ground temperature 0.04 m depth				
D110 (32.82° N, 93.01° E)	Mean annual	Seasonal amplitude	Bare ground	Vegetation	Texture (top soil)
Obs[h]			60–70 %	grass (Kobresia humilis)	coarse and fine sand
CLM4.5[b]	−1.8	1	33 %	7 % boreal_shrub 57 % C3 arctic grass	60 % sand 21 % clay
CoLM[c]	0.5	1.4	1 %	56 % C3 arctic grass 43 % C3 non arctic grass	45 % sand 17 % clay
ISBA[d]	−1.4	0.8	10 %	89 % C3 grass	50 % sand 11 % clay
JULES[j]	−1.9	0.9			
LPJ -GUESS[e,i]	−4.1	−3.7		tundra	clay-like
UVic[f]	1.1	−0.5	6 %	31 % C3 grass 60 % shrub	45 % sand 30 % clay

[a] Yang et al. (2000).

[b] https://dl.dropboxusercontent.com/u/41730762/surfdata_0.9x1.25_simyr1850_c130415.nc.

[c] Ji et al. (2014).

[d] Harmonized World Soil Database.

[e] Thermal diffusivities follow Van Duin (1963) and Jury et al. (1991), volumetric fraction of organic material follow Hillel (1998), water held below wilting point and porosity from AWFA (2002).

[f] Scholes and de Colstoun (2012) (http://www.daac.ornl.gov).

[g] Wang et al. (2012).

[h] Yang et al. (1999).

[i] The classification of soil texture is based on soil volumetric water holding capacity, thermal diffusivities, volumetric fraction of organic material, water held below wilting point and porosity.

[j] This model does not provide soil parameter information.

Table 5. Year-round relative model characteristics on TP.

Model	Snow cover[a]	Albedo[b]	Soil water[c]	Unfrozen water effect during phase change	Organic layer insulation effect
CLM4.5	Medium	Medium	Medium	yes	Yes
CoLM	Medium	Medium	Medium	no	No
ISBA	Low	Low	Medium	yes	Yes
JULES	Low	Low	Medium	yes	No
LPJ-GUESS	Medium	Low	High	no	No
UVic	None	Low	High	No	No

[a] Low snow cover is confined to high elevations, medium tends to be on western TP.
[b] LPJ-GUESS has constant albedo everywhere and UVic albedo varies slightly due to vegetation, year-round albedo variability for other models depends mainly on snow cover in winter and soil moisture, vegetation, etc in summer.
[c] Soil water content includes both liquid and ice fractions.
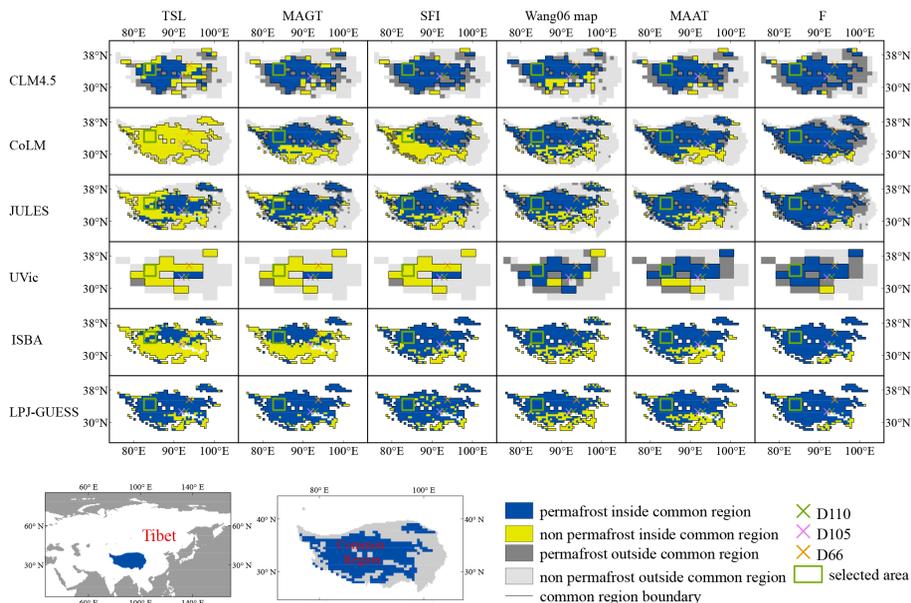
Figure 1. Permafrost maps derived from different diagnostic methods and models compared with Wang06 map. Permafrost inside the common modeling region is used for all-models inter-comparison, while permafrost outside allows further evaluation over the whole TP for CLM4.5, CoLM, JULES and UVic. The observation-based map of permafrost (Wang et al., 2006) is re-gridded to match model resolution.
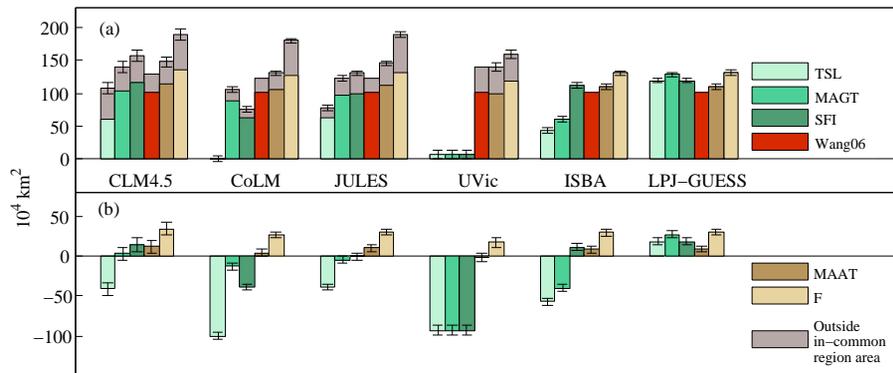
Figure 2. Permafrost areas derived from different diagnostic methods compared with Wang06 map. **(a)** Permafrost area, with TP permafrost outside the common region denoted by grey extensions to the bars for CLM4.5, CoLM, JULES and UVic. **(b)** Bias in permafrost area "Model minus Wang06 estimate", only for the common modeling region. Error bar is estimated from resolution differences.
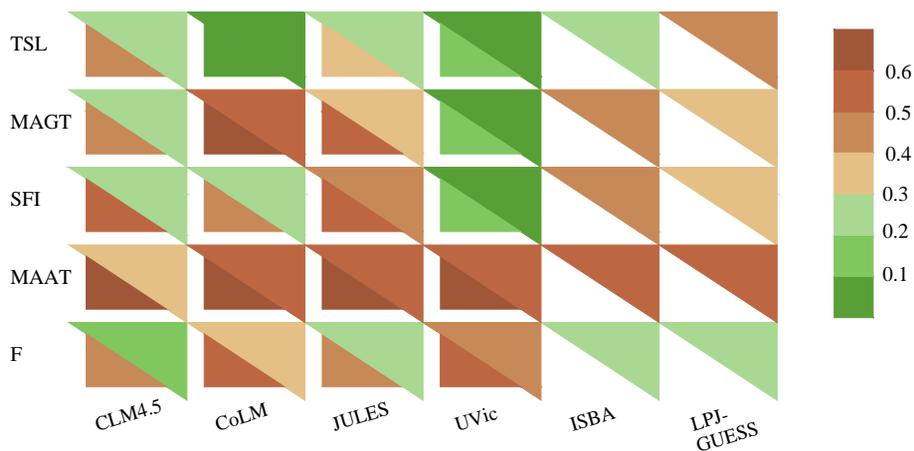
Figure 3. Kappa coefficient, K, quantifying the agreement between model-derived and Wang06 maps (see Sect. 3.3). $K \geq 0.2$ indicates at least fair agreement with Wang06 map. The lower triangle is K for the whole TP and is only available for CLM4.5, CoLM, JULES and UVic, while the upper triangle is K for the common modeling region.
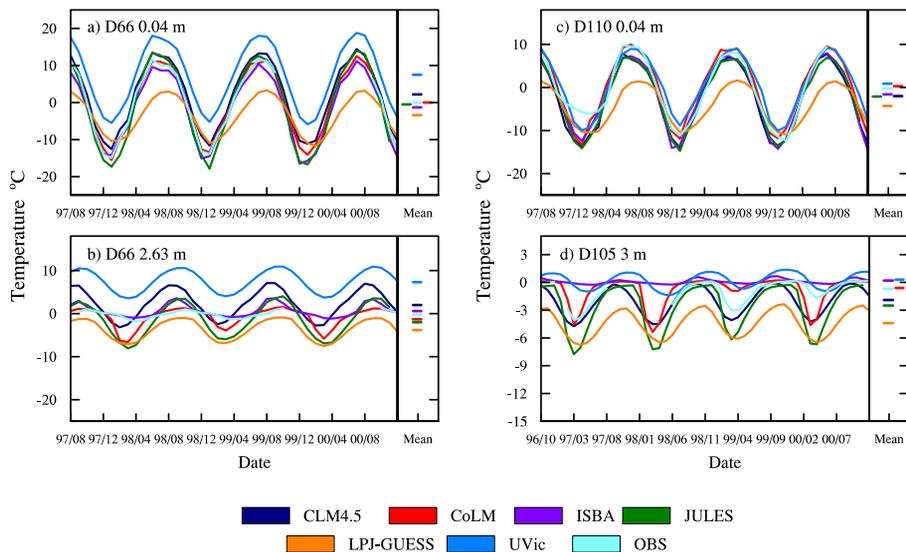
Figure 4. Monthly soil temperature variations at 3 stations from models and observations. **(a)** and **(c)** soil temperature of top layer. **(b)** and **(d)** soil temperature of deeper layer, 1996–2000. "Mean" denotes annual average temperature.
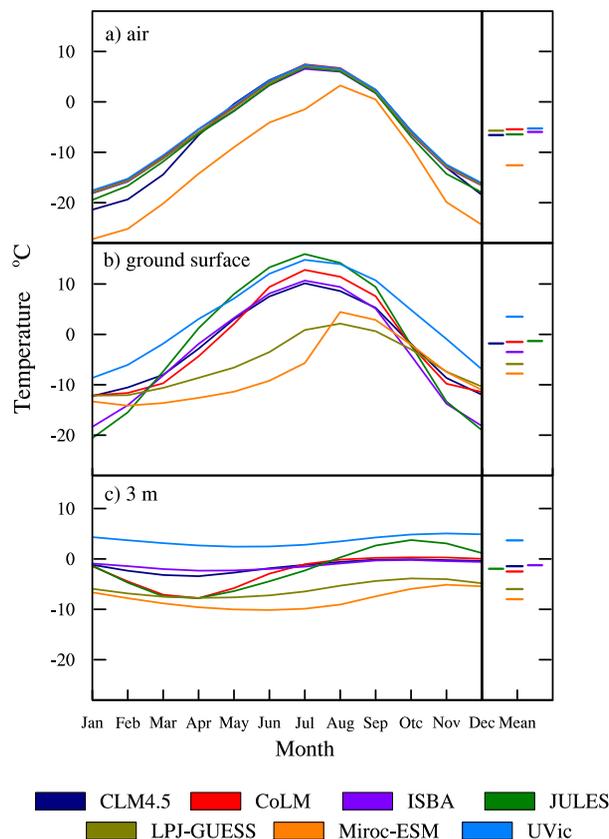
Figure 5. Monthly temperatures averaged over the selected western TP area in Fig. 1. **(a)** Forcing air temperature, **(b)** ground surface temperature, **(c)** 3 m soil temperature, averaged over 1980–2000. "Mean" denotes annual average temperature.
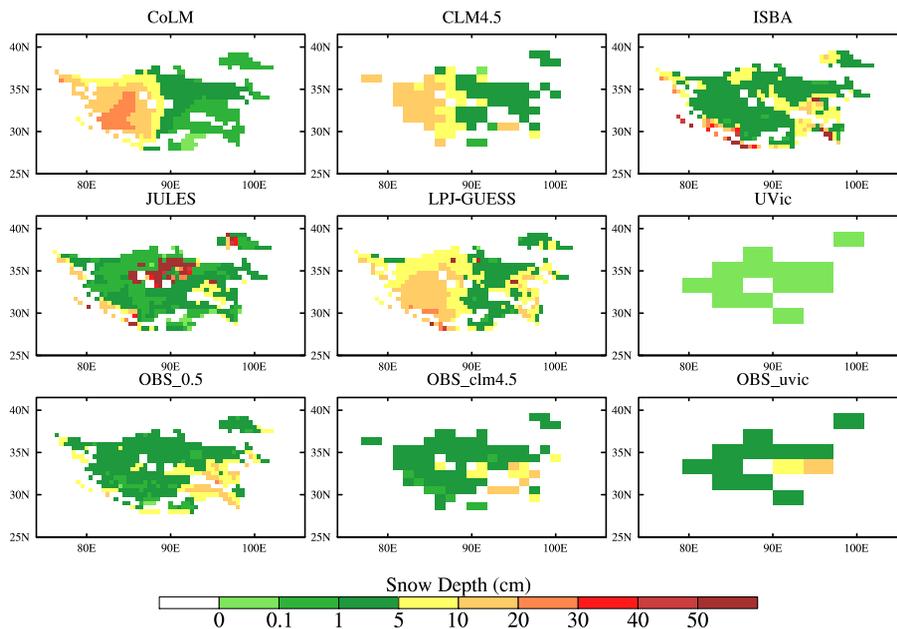
Figure 6. Winter snow depth for the common region, averaged over 1980–2000. Note the nonlinear color scale.
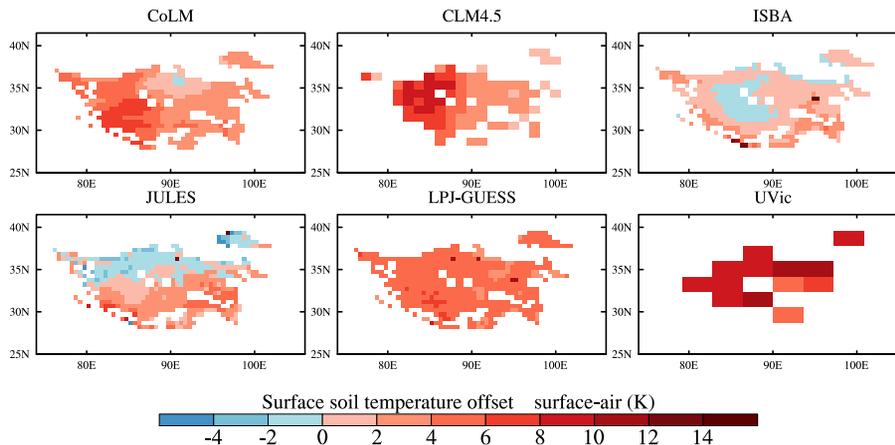
Figure 7. Mean surface temperature offset: difference in mean winter temperatures between surface soil and air, averaged over 1980–2000. Warm colors indicate soil is warmer than air temperature.
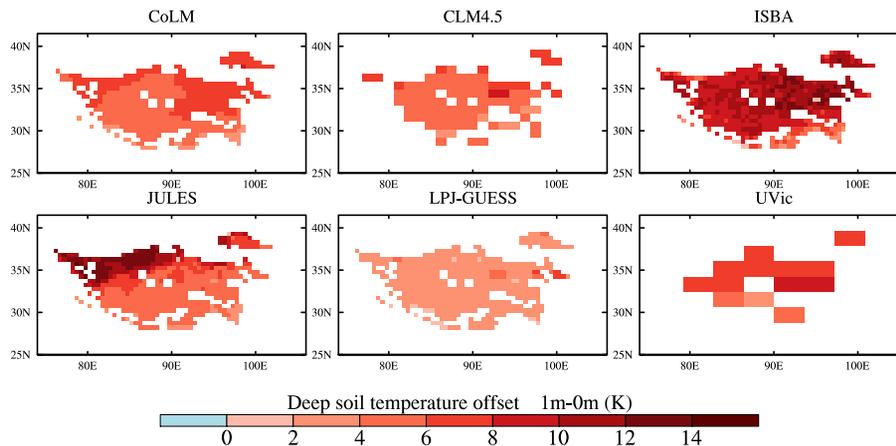
Figure 8. Mean soil temperature offset: difference in mean winter temperatures between soil at 1 m depth and surface soil, averaged over 1980–2000. Warm colors indicate deep soil is warmer than shallow soil.